Early stages of the Schottky barrier formation in submonolayer Pt on $SrTiO_3$ (001)

Hosung Seo* and Alexander A. Demkov†
Department of Physics, The University of Texas at Austin, Texas 78712, USA
(Received 13 September 2015; revised manuscript received 3 November 2015; published 4 December 2015)

We investigate the early stages of Pt nanocluster formation on $SrTiO_3$ (001) and the emergence of the Schottky barrier at the interface as a function of submonolayer Pt coverage using density functional theory. We find that there is a critical coverage of a 3/8 monolayer (ML), below which the Pt-oxygen interaction is dominant, leading to an ordered reconstructed surface with local Pt(II)-oxide structures. Beyond the critical coverage of 3/8 ML, the system undergoes a crossover at which the Pt-Pt interaction becomes dominant, leading to the formation of closed-packed hexagonal Pt nanoclusters. We show that cluster-induced gap states that pin the Fermi level at 1.3 eV above the valence band edge emerge at the same time as this crossover, thus showing the critical role it plays in determining the Schottky barrier height of the Pt/$SrTiO_3$ (001) interface.

DOI: 10.1103/PhysRevB.92.245301 PACS number(s): 73.20.−r

I. INTRODUCTION

Noble-metal nanoclusters on oxide substrates have attracted a significant amount of attention for their interesting electronic and structural properties [1–4] as well as their critical roles in technological applications, such as photocatalysis [5–7]. $SrTiO_3$ (STO) has been identified as a photocatalyst for hydrogen production via water splitting under zero bias [8–11]. The band gap of STO is 3.2 eV (UV active), and its conduction-band minimum is positioned about 4.0 eV below the vacuum level, matching up well with the redox potential of water [12]. However, the overall quantum efficiency is low, and a number of limiting factors have been intensively discussed in the literature [12,13]. In particular, a major challenge is to decrease the electron-hole recombination rates after they are created by a light irradiation. A possible solution to this problem is to design a suitable heterogeneous catalyst that can separate electrons and holes at the interface. Noble metals, such as Pt, are frequently loaded on titania as a cocatalyst to boost the catalytic activity of titania [8,14–18]. The enhanced catalytic activity has been attributed in part to the fact that Pt on STO forms a Schottky barrier [19–24] and that the rectifying behavior of this Schottky barrier may allow Pt nanoclusters on the oxide surface to trap electrons, effectively reducing the oxidants in a photocatalytic process [12,25]. However, although the interfacial electronic structure seems to play an important role in boosting the photocatalytic activity of Pt nanoclusters on STO, the process of formation of both the interface and the Schottky barrier is not well understood.

In this paper, we use density functional theory (DFT) to investigate the early stages of Schottky barrier formation in submonolayer Pt on the $SrTiO_3$ (001) surface. A crucial step for understanding the Schottky barrier of a metal-oxide system is to identify the character of the interface states responsible for charge transfer and thus the formation of the dipole layer at the interface [23,26]. Interestingly, previous photoemission studies on the Pt-STO system as a function of Pt coverage have indicated that the Schottky barrier formation is a rather continuous process [19–22], meaning that Pt-related interface states appear at the Fermi level and evolve even at a submonolayer (ML) coverage of Pt and that a sharp metallic feature at the Fermi level settles in at around one full monolayer coverage. It is worth noting that a similar continuous process of barrier formation has been explored in a number of submonolayer metal/semiconductor interfaces experimentally [27,28] and theoretically [29,30]. The character of the interface-induced gap states mediating interfacial charge transfer could be largely dependent on the dominant interaction at the interface and thus dependent on interfacial morphology. A limiting case is when a metallic overlayer wets an oxide surface, in which metal-oxygen bonding dominates the electronic and chemical interactions at the interface. In this case, the charge transfer and thus the Schottky barrier at the interface, can be determined mainly by considering the metal-oxygen chemical bonds [31]. An opposite limiting case is when metal-metal bonding dominates and metal-oxygen interactions are relatively weak or negligible. Thus, in the case of Pt, it is natural to consider the formation of metallic fcc nanocrystals on the surface of an oxide. The Fermi level of the metallic *d* band in such a system would be pinned by the charge neutrality level of the oxide [24,32].

Several DFT calculations have been previously reported that address the interface and Schottky barrier formation at the Pt/STO(001) interface [23,33–35]. Asthagiri and Sholl explored the favored arrangement of a Pt(001) monolayer on TiO_2-terminated STO(001) and found that Pt(001) prefers to adsorb on top of the oxygen sites, suggesting a coherent epitaxial Pt/STO(001) interface up to five Pt monolayers [33]. Mrovec *et al.* adopted the Pt/STO(001) structure suggested by Asthagiri and Sholl and calculated its *p*-type Schottky barrier to be 1.8 eV [23]. We note, however, that the (001) orientation of a Pt overlayer, which was the main assumption in the previous studies [23,33], may not be the most favorable structure of Pt on STO(001), and a disordered (111)-type Pt overlayer is more likely to occur based on our recent results [34,35]. It is also worth mentioning that researchers found interesting kinetics of Pt submonolayers on a number of different oxide surfaces, such as TiO_2 [36–38]. Therefore, a detailed study of the atomic structure of submonolayer Pt on STO and its effect on the emergence of in-gap states may provide a deeper understanding of Schottky barrier formation in dispersed Pt nanoparticles on STO.

*Current address: The Institute for Molecular Engineering, The University of Chicago, Chicago, Illinois 60637.
†demkov@physics.utexas.edu

For the Pt/STO (001) system, Christensen *et al.* reported interesting hierarchical nanoparticle morphology [39] where Pt at around one monolayer coverage aggregated to well-dispersed nanoparticles but without coalescence [39]. This result is intriguing, because, thermodynamically Pt would normally prefer to completely coalesce in order to minimize the Pt surface area as the surface energy of Pt is much higher than that of STO (001) [34,35]. It was argued that there might be some mechanism that kinetically hinders the thermodynamic forces, such as a chemical state of Pt or a physical barrier at a low Pt coverage [39]. This hierarchical Pt nanoparticle morphology is certainly beneficial to photocatalytic applications since the system could maintain a high surface-to-volume ratio. On the other hand, a subtle competition between Pt-Pt interaction and Pt-surface interaction might exist at a low coverage of Pt. Using atomic layer deposition and x-ray absorption spectroscopy, Christensen *et al.* have observed an evolution from Pt(II) oxide to metallic Pt and an increase in Pt-Pt bonding with a decrease in Pt-O bonding in the early stages of submonolayer Pt deposition [40].

To elucidate the subtle interplay between Pt-Pt and the Pt-STO interactions and its consequence on Schottky barrier formation in the submonolayer Pt/STO system, we theoretically investigate the early stages of Pt growth on TiO_2-terminated STO (001) and the emergence of in-gap states in the submonolayer Pt on that surface. The paper is organized as follows: In Sec. II, we summarize our computational methods. We present our main results in Sec. III, where we discuss the behavior of Pt monomer, dimer, and trimer structures on the TiO_2-terminated STO(001) surface; in Sec. IV, we summarize our main conclusions and discuss possible connections between our present theoretical results and the existing experimental results in the literature.

II. COMPUTATIONAL DETAILS

We use density functional theory within the local density approximation (LDA) as implemented in the VASP code [41]. The exchange-correlation functional is approximated using the parametrization of Ceperley-Alder data by Perdew and Zunger [42]. We employ projector augmented-wave pseudopotentials to describe Sr, Ti, O, and Pt [43], and a cutoff energy of 600 eV is used. Valence electron configurations for the elements are $4s^2\,4p^6\,5s^2$ for Sr, $3d^2\,4s^2$ for Ti, $2s^2\,2p^4$ for O, and $5d^9\,6s^1$ for Pt. Each self-consistent electronic calculation is converged within a 10^{-6} eV per cell, and the ionic relaxation is performed until the forces are less than 0.01 eV/Å. We use a supercell method to investigate the interaction between submonolayer Pt and STO (001). We model the TiO_2-terminated STO(001) surface using a four-unit-cell-thick STO slab with a 2×2 surface cell (lateral dimension of 7.75×7.75 Å^2). The STO (001) slab in the supercell is separated by a 16-Å-thick vacuum space from its next-nearest periodic images to avoid a spurious slab-slab interaction. For the ionic relaxation, we use a $4 \times 4 \times 1$ k-point grid. For selected configurations of 1/8- and 1/4-ML coverage of Pt on STO, we check that the main results remain unchanged as we change the cutoff energy and the k-point grid to 700 eV and $6 \times 6 \times 2$, respectively. The density of states (DOS) and total energy calculation, we use the $6 \times 6 \times 2$ k-point grid. To satisfy the periodic boundary condition along the c direction, the bottom STO surface is reconstructed in the same way as the top STO surface is. In other words, there is a mirror plane at the center of each supercell, and this is essential to properly describe the interfacial electronic structure.

III. RESULTS

A. Potential-energy surface for one Pt atom on STO (001)

We start our investigation by considering 1/8-ML coverage of Pt on the STO surface. This corresponds to one Pt on the 2×2 surface. The Pt-Pt bond length in the Pt bulk is 2.763 Å in our theory. Therefore the (2×2) surface is large enough, allowing us to consider the Pt adatom as a separate entity on the surface. We calculate the potential-energy surface (PES) for one Pt adatom, and it is shown in Fig. 1(a).

From the PES in Fig. 1(a), we note that Pt can be bound by surface O whereas Ti repels it. We also see that the O sites provide relatively shallow local minima, but Pt feels much stronger and has a deeper potential at the hollow site where Pt is maximally coordinated by four oxygen atoms on the surface. The energy barrier from the hollow site to the nearest O site is calculated to be 2.04 eV, whereas the barrier between the nearest-neighboring O sites is 0.46 eV. To estimate the time scale for Pt diffusion, we use the Arrhenius formula for kinetics $1/\tau = \nu e^{-E/k_B T}$, where τ is a time interval between Pt hopping, E is the energy barrier for hopping, and ν is an attempt frequency [44]. Assuming $\nu \approx 10^{12}$ s^{-1} [45], the time scales for hopping at room temperature are on the order of microseconds and 10^{22} s for the case of the O site to the O site and that of the hollow site to the O site, respectively. Therefore, a Pt adatom is highly mobile on most of the STO (001) surface

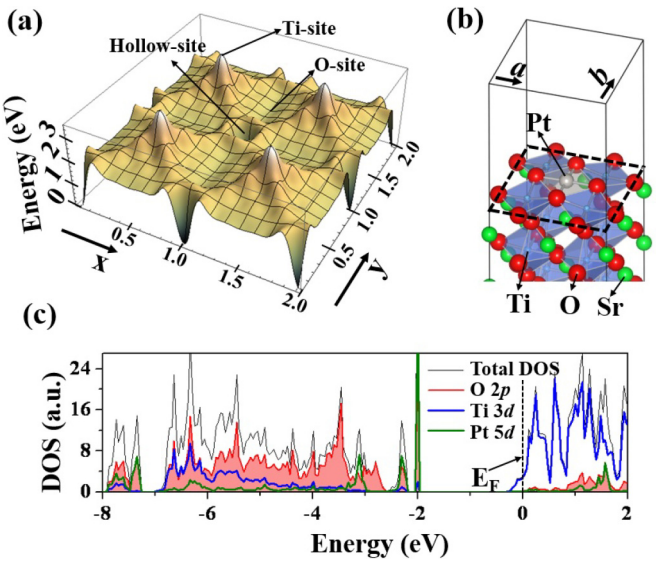

FIG. 1. (Color online) (a) The PES for a Pt adatom on the $2a \times 2a$ STO surface, where a is the STO lattice constant. The lowest energy is set at 0 eV. The spatial resolution is 0.48 Å. (b) The lowest-energy structure for the 1/8-ML coverage of Pt on STO (001). (c) Projected density of states of the $PtTi_4O_8$ surface layer shown in (b). The Fermi energy (E_F) is shown as a dashed vertical line.

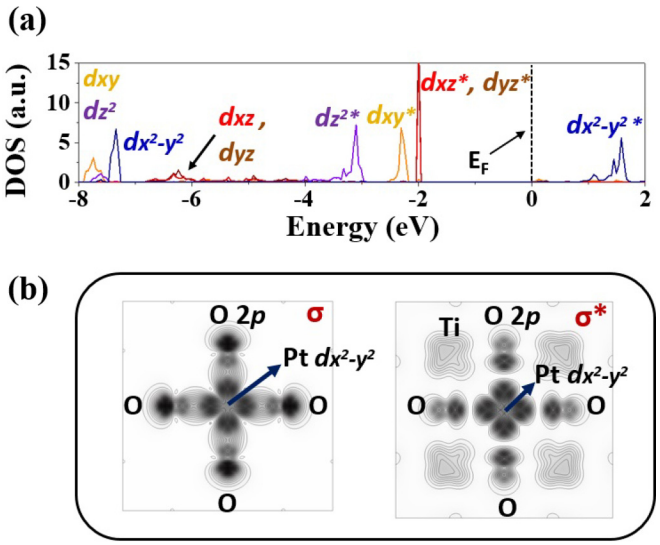

FIG. 2. (Color online) (a) The orbital-projected Pt density of states and (b) density plots of bonding and antibonding states between Pt 5*d* and O 2*p* orbitals of the $PtTi_4O_8$ surface shown in Fig. 1.

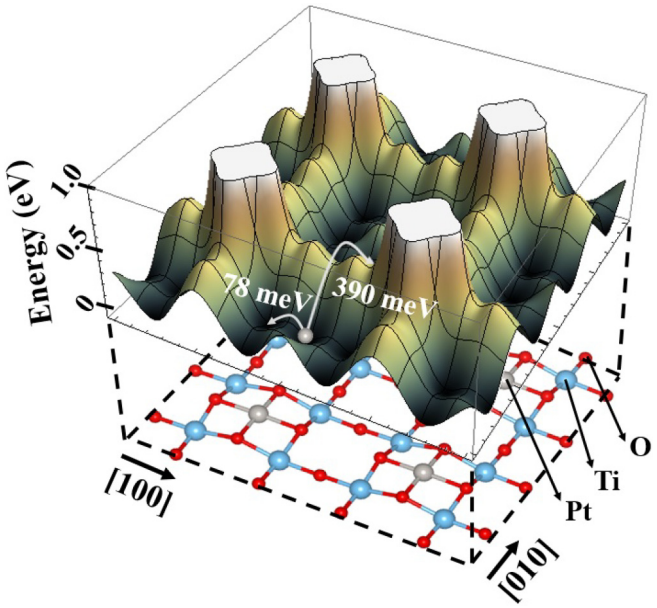

FIG. 3. (Color online) The PES for Pt on the PTO surface [see Fig. 1(b)]. The size of the PES plot is $4a \times 4a$, where a is the STO lattice constant A schematic of the surface structure drawn under the PES. The spatial resolution for the PES calculation is 0.96 Å. The saturation level for the plot is set at 1.0 eV, above which the PES is not shown (plateau areas around the Pt sites).

area, but if Pt is trapped at the hollow site, it cannot escape by itself.

Interestingly, Pt captured at the hollow site not only maximizes the coordination number by O, but also sinks down into the surface as shown in Fig. 1(b), forming a PtO-like local oxide structure in a square-planar geometry [40,46–48]. In Fig. 1(c), we plot the projected density of states of the surface TiO_2 layer with adsorbed Pt. It is clearly seen that fivefold degenerate atomic *d* states of Pt split and resonate in energy with surface O 2*p* states due to the bonding interaction. In Fig. 2, we show some of these bonding and antibonding orbitals. We find the Pt-O bond length to be 2.01 Å that is close to 2.04 Å of the PtO bulk [46,47] and to 1.98 Å of PtO formed on the STO(001) surface [40]. We calculate the amount of charge transfer from Pt to O using the Bader charge analysis [49,50] to be 0.83*e* that is also close to 0.86*e* in bulk PtO [48]. In the presence of the PtO structure, the surface stoichiometry is $PtTi_4O_8$. Assuming the nominal oxidation state of 2+ for Pt in PtO, Ti on the reconstructed surface would have the oxidation state of 3.5+. This feature gives rise to a metallic surface due to the partial occupation of the bottom of the conduction band originating from the Ti $3dt_{2g}^*$ states as shown in Fig. 1(c). We will call this surface $PtTi_4O_8$ (PTO) for the rest of this paper.

B. Pt clusters

Next, we consider the interaction between additional Pt atoms on the reconstructed PTO surface. We first check that, if there is a Pt_2 dimer on the clean STO (001) surface, it is energetically favorable to break the dimer bond and form the two local PtO structures separated by a hollow site. In Fig. 3 we plot the PES for a second incoming Pt on the PTO surface. A noticeable feature is that the nearest-neighbor hollow sites of a PtO structure do not bind the second Pt atom. It means that, at the Pt coverage of 1/8 ML, the TiO_2 surface is fully saturated by the local PtO structures. It is also interesting that the PtO structures provide large kinetic barriers for the Pt diffusion. In addition to the enormous barrier around the hollow site trapping a Pt atom, crossing the barrier present between the local PtO structures requires 390 meV as shown in Fig. 3. In addition, we remark that now the Ti sites are able to bind Pt, which was not possible on the clean STO(001) surface as shown in Fig. 1(a). The Pt-Ti binding is a metallic bond, and it is possible as Ti in the PTO surface has partial electron occupation [see Fig. 1(c)]. Setting the binding energy of Pt on the O site to be 0.0 meV, the binding energy of Pt on the Ti site is only 6 meV higher in energy, and the diffusion barrier between the O and the Ti sites is calculated to be 78 meV as shown in Fig. 3.

To find the lowest-energy Pt nanostructure at the coverage of 3/8 ML, we consider 25 different initial configurations of Pt based on the low-energy structures from the 2/8-ML Pt configurations. We first consider all possible configurations of dispersed Pt atoms adsorbed on top of the O and Ti sites that are identified as the binding sites of the PES in Fig. 3. However, there is always a 3–5-eV energy gain when Pt dimerizes in the square potential well shown in Fig. 3. We show the lowest-energy Pt dimer structure on the PTO surface in Fig. 4 (a). The Pt-Pt bond length is calculated to be 2.47 Å that agrees with a theoretical bond length of the Pt dimer of about 2.4 Å in a gas phase [51]. Next, we consider a Pt trimer on the clean TiO_2 surface, and the lowest-energy structure is shown in Fig. 4(b). Interestingly, there is an energy gain of 150 meV, compared to that in the Fig. 4(a). We also check that, if the Pt dimer in Fig. 4(a) is brought on top of the PtO structure, then subsequent structural relaxation destabilizes the PtO structure and a Pt trimer is formed on the surface. We note that Pt_3 no longer follows the surface symmetry as shown in Fig. 4(b). Instead,

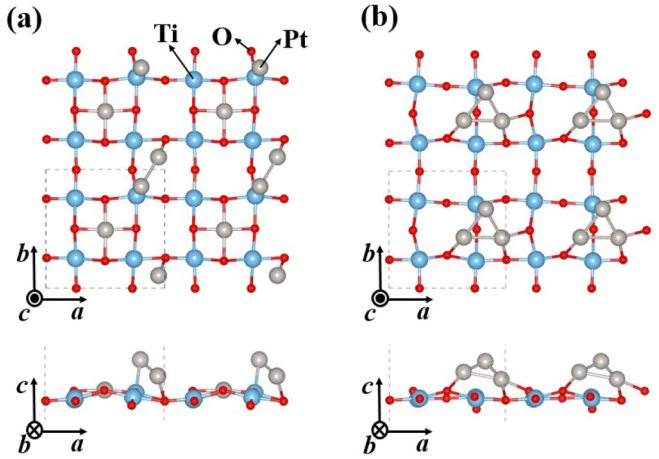

FIG. 4. (Color online) Low-energy surface structures for the 3/8-ML coverage of Pt on STO (001). (a) Pt dimer on the reconstructed PTO surface and (b) Pt trimer on the TiO_2 surface. The STO structure below the surface TiO_2 layer is not shown for clarity. The surface unit cell is indicated by the dashed line. The upper (lower) picture is a top (side) view.

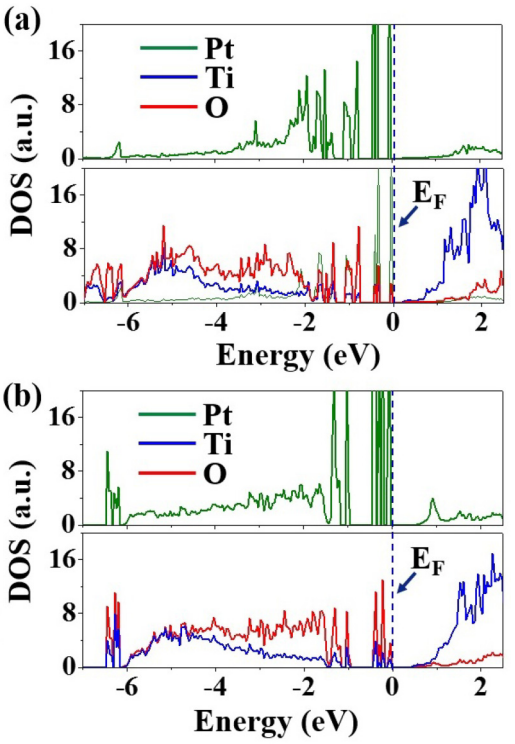

FIG. 5. (Color online) Atom-projected density of states of (a) the Pt dimer on the PTO surface and (b) the Pt trimer on the TiO_2 surface. The upper panels are for (a) the adsorbed Pt dimer or trimer and the surface electronic structures are shown in the lower panels. The Fermi energy is set at 0 eV.

it has a triangular structure, which is a motif of a closed-pack-hexagonal structure of the Pt (111) layer. We calculate the bond lengths and angles to be varying from 2.47 to 2.55 and from 59° to 62°, respectively, that closely follow the Pt trimer structure in a gas phase [51]. The trimer structure is also not planar on the surface because the Ti site now tends to repel Pt on top of it.

In Figs. 5(a) and 5(b), we show the atom-projected density of states calculated using the structures shown in Figs. 4(a) and 4(b), respectively. We note that structural transition from the dimer in Fig. 4(a) to the trimer structure in Fig. 4(b) is driven by the stronger metallic Pt-Pt interaction in the Pt trimer [51] than the Pt-oxide interaction mediated by the surface oxygen. Comparing Figs. 5(a) and 5(b), we observe that the structural transition creates a significant number of states near the Fermi level in the band gap of STO. Our results show that interface-induced states in the STO gap start to appear even at the submonolayer Pt coverage and metallicity in the Pt nanoclusters also start to develop as manifested by the appearance of the large metallic d-band-like DOS below the Fermi level. By considering the pDOS of the middle STO layer of the cell (not shown), we find that the Fermi level is pinned at 1.3 eV above the STO valence-band top, which is the same as the charge neutrality of STO calculated by Demkov *et al.* using the complex band structure of STO [32]. We will further show that the Fermi level of a full monolayer Pt-STO (001) structure is also pinned at 1.3 eV above the STO valence-band top. The Fermi-level pinning for the Pt_3 trimer is intriguing because the Pt_3 trimer is not truly metallic with a full metallic d band by itself. The minimum distance between the Pt trimer and it nearest-neighbor image trimer in Fig. 4(b) is 5.3 Å, meaning that the direct Pt trimer-trimer interaction is negligible. So, technically speaking, they are cluster-induced gap states. It is also very interesting to see that the states near the Fermi level in the STO gap have the orbital character of both Ti and O. We note that the evanescent states in the gap change their character from valencelike to conductionlike as a function of the Fermi-level position in the gap. Therefore, since the Fermi level is pinned at the branch point of the complex band, which is the charge neutrality level, the states at the Fermi level have both the conduction (mostly Ti $3d$ states) and the valence (mostly O $2p$ states) characters as shown in Fig. 5(b).

To calculate the Schottky barrier of a full Pt monolayer on STO (001), we consider a number of Pt (001) and Pt(111) monolayer geometries on STO(001). We find the lowest-energy structure of a monolayer Pt(001) configuration is one in which all the Pt atoms are bound by the surface oxygen atoms [34], which is consistent with previous calculations [33]. To consider Pt(111) on STO(001), we use a $\sqrt{2}a \times 2\sqrt{2}a$ surface cell [Fig. 6(a)], where a is the STO lattice constant. After matching Pt(111) to the surface cell, we translate the Pt(111) sheet over the surface and find the lowest-energy structure, which is shown in Fig. 6(a). We note that there is a small lattice mismatch between Pt and STO of 0.9% in theory and 0.5% in experiment. So, the Pt(111) sheet shown in Fig. 6(a) is slightly strained along the b direction, and it is free to relax in the a direction. In addition, the Pt(111) sheet should be free to rotate in principle, but it is not allowed in our calculations due to the surface cell size and the periodic boundary condition. We argue, however, that the dominant interaction at the full monolayer Pt coverage would be the Pt-Pt metallic interaction as discussed for the Pt_3 trimer structure on STO. Therefore, the Pt(111) structure that is considered in Fig. 6(a) would capture the essential feature of the interfacial

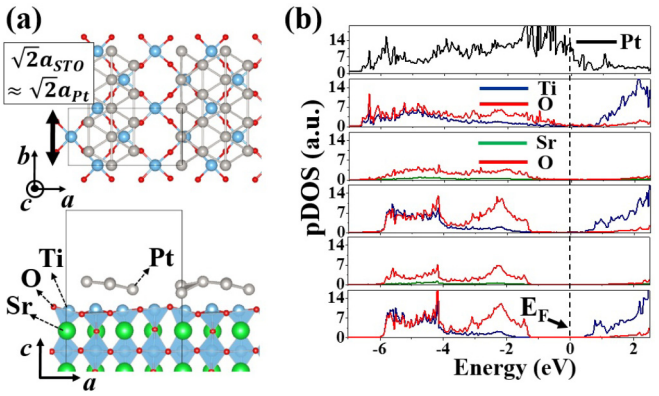

FIG. 6. (Color online) (a) Schematic of a full monolayer of Pt(111) on the TiO_2-terminated STO(001) surface viewed from the top (up) and the side (bottom). The top TiO_2 layer and the Pt(111) sheet are only visible in the top view for clarity. (b) The layer-by-layer projected density of states of the Pt(111)/STO(001) structure. The Fermi level is pinned at 1.3 eV above the valence-band top of the bulk STO.

electronic structure and charge-transfer property through the metal-induced gap states (MIGS) in STO.

We first note that the energy of the Pt(111) structure shown in Fig. 6(a) is lower than that of the lowest Pt(001) structure by 0.43 eV per Pt atom. This is consistent with our previous conclusion that, beyond the 3/8-ML Pt coverage, Pt nanoclusters on STO(001) do not follow the surface (1×1) symmetry but prefer to form Pt(111) hexagonal structures. We show the layer-by-layer pDOS of the Pt(111)/STO(001) system in Fig. 6(b). We observe that the monolayer Pt(111) sheet exhibits a full metallic *d* band and it transfers electrons to the evanescent gap states in STO. Additionally, the charge transfer rapidly decays within the two unit cells of STO, and the bulk electronic structure of STO is recovered in the middle of the supercell, which is consistent with the complex band-structure calculations [32]. We calculate the Fermi level to be pinned at 1.3 eV above the valence-band top, which is the same for the Pt_3 cluster on STO(001) as shown in Fig. 5(b). By considering the experimental STO band gap of 3.2 eV, we calculate the *n*-type Schottky barrier height between the Pt(111) sheet and the STO(001) to be 1.9 eV. Our results suggest that the Fermi-level pinning, thus the emergence of the Schottky barrier in the Pt nanocluster/STO system, is controlled by the evanescent states of the bulk STO and it appears when the Pt-Pt metallic interaction becomes dominant over the Pt-surface interaction, which is consistent with the previous experimental observations [19,40].

IV. DISCUSSIONS AND CONCLUSION

In conclusion, we have theoretically investigated the early stages of the interface and Schottky barrier formation in submonolayer Pt on $SrTiO_3$ (001). We found that there is a drastic change in the nature of bonding of Pt on STO as a function of Pt coverage. At a low coverage below 2/8 ML, the dominant interaction is Pt-O chemical bonding with Ti atoms repelling Pt, leading to the formation of local Pt(II) oxide structures on the surface. In the presence of the local PtO structures, however, the Ti sites are able to bind Pt through a metallic bonding. Upon increasing the Pt coverage, metallic Pt-Pt interaction becomes dominant, and hexagonal Pt(111) nanocrystals start to form, making the interaction between the Pt and the oxide surface neither directional nor site specific. We note that our finding is consistent with the experimental results reported by Christensen *et al.*, who used atomic layer deposition and x-ray absorption spectroscopy and observed a progression from the Pt(II) oxide to metallic Pt as the Pt coverage on STO(001) is increased [40]. Additionally, our results indicate that at a low coverage of Pt on STO(001), the local PtO structures can provide kinetic barriers, which may play a role in hindering the complete coalescence of the Pt nanostructure and help retain a high surface-to-volume ratio [39]. This high surface-to-volume ratio should be advantageous for low-coverage Pt on STO to be used as an efficient photocatalyst.

We also showed that the formation of the Schottky barrier is a continuous process [19–22]. We found that interface-induced gap states pinning the Fermi level start to appear in the STO band gap even at submonolayer Pt coverage and that the emergence of the gap states is directly associated with the change in the dominant interaction on the surface. We also showed that at a coverage below 3/8 ML of Pt, Pt-O chemical bonding, which leads to the formation of local Pt(II) oxide structures, controls the Fermi level position. However, above this critical coverage of 3/8 ML, the system starts to develop interface-induced gap states as the Pt-Pt metallic bonding starts to dominate, with Pt preferring to arrange as (111) hexagonal nanocrystals. The cluster-induced gap states pin the Fermi level 1.3 eV above the STO valence-band top. We also showed that the Fermi level of a full metallic Pt(111) monolayer is pinned at the same energy by the same evanescent MIGS. Based on the MIGS theory, the STO pinning factor *S* is 0.28 using the dielectric constant of STO [24], suggesting a moderate Fermi-level pinning at metal/STO interfaces. Therefore, our results suggest that the pinning level of 1.3 eV at the Pt/STO(001) interface is close to the charge neutrality level of STO, which is consistent with the estimate of Demkov *et al.* [32].

We calculate the *n*-type Schottky barrier of the Pt/STO(001) interface to be 1.9 eV by subtracting the *p*-type Schottky barrier of 1.3 eV from the experimental band gap of STO, which is 3.2 eV. We use the experimental band gap as the theoretical value is only 1.7 eV, due to the well-known band-gap underestimation inherent to (semi-)local exchange-correlation functionals, such as LDA or generalized gradient approximation [52]. The application of higher-level theories, such as *GW* many-body perturbation theory [53] or properly tuned Hartree-Fock hybrid functional theory [54] to Pt/dielectric oxide systems [55] may result in an improved prediction of the *n*-type Schottky barrier heights of these and related heterogeneous photocatalytic systems. We also emphasize the importance of an explicit interface calculation as the detailed structure of the interface controls the charge transfer, and thus the charge neutrality level and the pinning strength in the MIGS theory.

We also note that there are still unresolved issues with the mechanism of Schottky barrier formation at the Pt/STO(001) interface, which we leave for future study. For example, we calculated the *p*-type Schottky barrier height of the metastable Pt(001) overlayer on STO(001) to be 1.8 eV, and this is in good agreement with the previous results of Mrovec *et al.* [23]. Experimentally, Schafranek and co-workers [19] measured the

n-type Schottky barrier heights for the $SrTiO_3$:Nb/Pt interface to be 1.5 and 0.6 eV for the oxidized and reduced interfaces, respectively, which are converted to 1.7- and 2.6-eV *p*-type Schottky barrier heights by using the 3.2-eV band gap of STO. It seems that the experimental value of 1.7 eV for the oxidized interface is in good agreement with the theoretical result of 1.8 eV that is obtained from the metastable epitaxial Pt(001) overlayer on STO(001). We note, however, that this does not necessarily mean that the Pt(001) overlayer is the structure observed in experiment, but that the situation could be more complex [19] and should be further investigated in the future.

We thank A. Posadas for a critical reading of the paper and helpful discussions. H.S. gratefully acknowledges support from the University of Texas at Austin through a William Powers, Jr., Presidential Fellowship. A.D. is grateful for support by the Air Force Office of Scientific Research under Grant No. FA9550-12-10494.

[1] F. Silly and M. R. Castell, Phys. Rev. Lett. **96**, 086104 (2006).
[2] N. Nilius, M. V. Ganduglia-Pirovano, V. Brázdová, M. Kulawik, J. Sauer, and H.-J. Freund, Phys. Rev. Lett. **100**, 096802 (2008).
[3] Z. Novotný, G. Argentero, Z. Wang, M. Schmid, U. Diebold, and G. S. Parkinson, Phys. Rev. Lett. **108**, 216103 (2012).
[4] Q. Fu and T. Wagner, Surf. Sci. Rep. **62**, 431 (2007).
[5] M. S. Chen and D. W. Goodman, Science **306**, 252 (2004).
[6] G. N. Vayssilov *et al.*., Nature Mater. **10**, 310 (2011).
[7] M. Kitano, K. Tsujimaru, and M. Anpo, Top. Catal. **49**, 4 (2008).
[8] R. G. Carr and G. A. Somorjai, Nature (London) **290**, 576 (1981).
[9] F. T. Wagner, S. Ferrer and G. A. Somorjai, Surf. Sci. **101**, 462 (1980).
[10] F. T. Wagner and G. A. Somorjai, J. Am. Chem. Soc. **102**, 5494 (1980).
[11] F. T. Wagner and G. A. Somorjai, Nature (London) **285**, 559 (1980).
[12] X. Chen, S. Shen, L. Guo, and S. S. Mao, Chem. Rev. **110**, 6503 (2010).
[13] M. R. Hoffman, S. T. Martin, W. Y. Choi, D. W. Bahnemann, Chem. Rev. **95**, 69 (1995).
[14] A. Paracchino, V. Laporte, K. Sivula, M. Grätzel, and E. Thimsen, Nature Mat. **10**, 456 (2011).
[15] S. Ikeda *et al.*, Catal. Today **117**, 343 (2006).
[16] B. Sun, A. V. Vorontsov, and P. G. Smirniotis, Langmuir **19**, 3151 (2003).
[17] J. A. Enterki, K. R. Poeppelmeier, and L. D. Marks, Nano Lett. **11**, 993 (2011).
[18] J. A. Enterkin, W. Setthapun, J. W. Elam, S. T. Christensen, F. A. Rabuffetti, L. D. Marks, P. C. Stair, K. R. Poeppelmeier, and C. L. Marshall, ACS Catal. **1**, 629 (2011).
[19] R. Schafranek, S. Payan, M. Maglione, and A. Klein, Phys. Rev. B **77**, 195310 (2008).
[20] M. Copel, P. R. Duncombe, D. A. Neumayer, T. M. Shaw and R. M. Tromp, Appl. Phys. Lett. **70**, 3227 (1997).
[21] Y. W. Chung and W. B. Weissbard, Phys. Rev. B **20**, 3456 (1979).
[22] M. K. Bahl, S. C. Tsai, and Y. W. Chung, Phys. Rev. B **21**, 1344 (1980).
[23] M. Mrovec, J.-M. Albina, B. Meyer, and C. Elsässer, Phys. Rev. B **79**, 245121 (2009).
[24] J. Robertson and C. W. Chen, Appl. Phys. Lett. **74**, 1168 (1999).
[25] J. S. Jang, H. G. Kim, and J. S. Lee, Catal. Today **185**, 270 (2012).
[26] M. K. Niranjan, L. Kleinman, and A. A. Demkov, Phys. Rev. B **77**, 155316 (2008).
[27] M. Prietsch, M. Domke, C. Laubschat, and G. Kaindl, Phys. Rev. Lett. **60**, 436 (1988).
[28] K. Stiles and A. Kahn, Phys. Rev. Lett. **60**, 440 (1988).
[29] A. Zunger, Phys. Rev. B **24**, 4372 (1981).
[30] J. Ortega and F. Flores, Phys. Rev. Lett. **63**, 2500 (1989).
[31] R. T. Tung, Phys. Rev. Lett. **84**, 6078 (2000).
[32] A. A. Demkov, L. R. C. Fonseca, E. Verret, J. Tomfohr, and O. F. Sankey, Phys. Rev. B **71**, 195306 (2005).
[33] A. Asthagiri and D. S. Sholl, J. Chem. Phys. **116**, 9914 (2002).
[34] H. Seo, A. B. Posadas, and A. A. Demkov, J. Vac. Sci. Technol., B: Nanotechnol. Microelectron.: Mater., Process., Meas., Phenom. **30**, 04E108 (2012).
[35] K. D. Fredrickson, A. B. Posadas, A. A. Demkov, C. Dubourdieu, and J. Bruley, J. Appl. Phys. **113**, 184102 (2013).
[36] H. Iddir, S. Öğüt, N. D. Browning, and M. M. Disko, Phys. Rev. B **72**, 081407(R) (2005).
[37] H. Iddir, V. Skavysh, S. Öğüt, N. D. Browning, and M. M. Disko, Phys. Rev. B **73**, 041403(R) (2006).
[38] T. Chang, Y. Tanaka, R. Ishikawa, K. Toyoura, K. Matsunaga, Y. Ikuhara, and N. Shibata, Nano Lett. **14**, 134 (2014).
[39] S. T. Christensen, B. Lee, Z. Feng, M. C. Hersam, and M. J. Bedzyk, Appl. Surf. Sci. **256**, 423 (2009).
[40] S. T. Christensen, J. W. Elam, F. A. Rabuffetti, Q. Ma, S. J. Weigand, B. Lee, S. Seifert, P. C. Stair, K. R. Poeppelmeier, M. C. Hersam, and M. J. Bedzyk, Small **5**, 750 (2009).
[41] G. Kresse and J. Furthmüller, Phys. Rev. B. **54**, 11169 (1996).
[42] J. P. Perdew and A. Zunger, Phys. Rev. B **23**, 5048 (1981).
[43] P. E. Blöchl, Phys. Rev. B **50**, 17953 (1994).
[44] H. Brune, Surf. Sci. Rep. **31**, 125 (1998).
[45] L. Xu, G. Henkelman, C. T. Campbell, and H. Jónsson, Surf. Sci. **600**, 1351 (2006).
[46] W. J. Moore and L. Pauling, J. Am. Chem. Soc. **63**, 1392 (1941).
[47] J. R. McBride, G. W. Graham, C. R. Peters, and W. H. Weber, J. Appl. Phys. **69**, 1596 (1991).
[48] N. Seriani, Z. Jin, W. Pompe, and L. Colombi Ciacchi, Phys. Rev. B **76**, 155421 (2007).
[49] R. F. W. Bader, *Atoms in Molecules: A Quantum Theory* (Oxford University Press, Oxford, 1990).
[50] W. Tang, E. Sanville, and G. Henkelman, J. Phys.: Condens. Matter **21**, 084204 (2009).
[51] P. Bloński, S. Dennler, and J. Hafner, J. Chem. Phys. **134**, 034107 (2011).
[52] J. P. Perdew and M. Levy, Phys. Rev. Lett. **51**, 1884 (1983).
[53] M. Govoni and G. Galli, J. Chem. Theory Comput. **11**, 2680 (2015).
[54] J. H. Skone, M. Govoni, and G. Galli, Phys. Rev. B **89**, 195112 (2014).
[55] C. Cazorla and M. Stengel, Phys. Rev. B **85**, 075426 (2012).